Review

Martin Rhême*, John Botsis, Joël Cugnoni and Parviz Navi

Influence of the moisture content on the fracture characteristics of welded wood joint. Part 2: Mode II fracture

Abstract: As a second part of this series, the present study also addresses the water resistance of joints obtained by friction welding. Here, the mode II fracture is in focus, that is, 4-points end-notched flexure specimens (4-ENF) were investigated with various moisture contents (MCs). The critical energy release rate was decreasing at higher MCs. The maximal shear strength of the joining material, as determined by torsion tests, was also affected by high MCs. The experimental data were implemented in a finite element model (FEM) based on the cohesive law to simulate the behavior of welded connection in 4-ENF tests. The FEM results describe well the experimental load-displacement curves.

Keywords: beech (*Fagus sylvatica*), cohesive law, finite element model (FEM), fracture mechanics, friction welding, mode II, moisture content (MC)

*Corresponding author: **Martin Rhême,** Material and Wood Technologies, Bern University of Applied Science, Bienne, Switzerland, e-mail: martin.rheme@bfh.ch
John Botsis and Joël Cugnoni: Laboratory of Applied Mechanics and Reliability Analysis, EPFL, Lausanne, Switzerland
Parviz Navi: Material and Wood Technologies, Bern University of Applied Science, Bienne, Switzerland

Introduction

The fracture characteristics of welded wood joints at different moisture contents (MC) are the focus of this investigation consisting of two parts. Part 1 (Rhême et al. 2013) reviews friction welding and the negative effect of moisture on welded wood joints, and the experimental part of Part 1 deals with the mode I fracture (opening mode). The present work describes the mode II fracture as a function of MC, which was not yet described in the literature. Mode II is a sliding mode fracture, in which the shear stress is acting parallel to the plane of the crack and perpendicular to the crack front. The expectation was that the mode II investigation will enlighten the additional aspects of the behavior of welded wood in the presence of moisture.

The mode II fracture of plain wood and wood joined with conventional adhesives is already well documented (Yoshihara 2012). End-notched flexure specimens (ENF) are well suited for the observation of mode II fracture because the crack propagation is usually stable. The RILEM TC 133 report (Aicher et al. 1997) gives a good overview of the early works for the determination of fracture energy (G_f) with the help of a tapered ENF. In this work, the specimens were investigated in the opening mode after crack propagation based on 3-points bending tests (3-ENF). The differences in fracture surfaces morphology enabled to measure the length of crack propagation in mode II and therefore G_f. Dry specimens (MC<5%) showed unstable fracture. Non-tapered specimens were also studied with either 3-points or 4-points bending (4-ENF) tests. The former leads to stable crack propagation only when the ratio "initial crack length/half-span length" is >0.7 (Yoshihara 2004, 2005, 2012). The 3-ENF is a convenient simple setup to measure G_{II} at crack propagation initiation, and the method was also applied for wood adhesive joints (Simon 2001; Kutnar et al. 2008; Arrese et al. 2010). Nevertheless, the performance of 4-ENF test is better due to a resulting longer zone of stable crack propagation. In composites, Schuecker and Davidson (2000) demonstrated the utility of 4-ENF tests for G_{IIc} measurements. G_{IIc} can only be computed reliably if the crack length can be measured several times with sufficient precision during crack propagation.

The effect of MC on fracture has received limited attention in the literature. In this context, Kretschmann and Green (1996) provided an expression that gives the critical stress intensity factor (K_{IIc}) of centered-slit beam specimens made of pine as a function of the MC. The maximal values were obtained at MCs between 7% and 13%.

The present work describes the specimen preparation by friction welding for 4-ENF and torsion tests. The measured

G_{IIc} and maximal shear strength obtained at different MC will form the basis for the numerical simulation of the behavior of the welded specimen. The effects of friction on the results of numerical simulations will also be considered.

Materials and methods

Specimen preparation

ENF specimens

The specimen preparation from *Fagus sylvatica* and their welding parameters were similar to that of the DCB specimen presented in Part 1 (Rhême et al. 2013). Grease was applied on the surface to avoid welding and permit to create the initial crack starter at 95 mm. The methodology to obtain samples with determined equilibrium MCs (EMCs) was also the same as in Part 1. The control specimens were submitted to the same treatment as that of 4-ENF specimens and were weighted periodically until the EMC was reached. The following MCs were obtained: 6.1%, 11.9%, 16.8%, and 22.1%. To avoid friction between the specimen and the supports, the supports were mounted on roller bearings. To impede the specimens from sliding away, a metallic wedge with a triangular section was glued on one of the beam's extremities. A specially designed roller prevented the specimens sliding during loading (Figure 1a and b). Before the test, the initial

crack tip position is grown up to 100 mm by inserting a razor blade between the wood beams. This step should sharpen the initial crack tip and facilitate the crack growth.

Torsion specimens

The torsion specimens are prepared with a plug cutter from the other half of the welded piece used for tension measurements (Rhême et al. 2013). The dimensions of the welded specimens are $500 \times 20 \times 60$ mm³. Thus, the cylindrical specimens with a 15 mm radius were manufactured so that the weld is situated at the middle of the 60-mm-long specimen (Figure 1c). Afterward, four groups of eight specimens each were stored in the climatic box and weighted. One day before the testing, the mass and exact dimensions of the specimens were determined. Then, they were left in the climatic box for one more day. Due to the anisotropic swelling, the section of the specimens at EMC is not circular but rather slightly elliptical; thus, the dimensions of the two principal axes were measured and used in the shear stress calculation.

Experimental methods

Fracture testing

The 4-point ENF test is performed on a uniaxial testing machine (Instron 5848 Microtester; Instron, Norwood, MA, USA) with a 2 kN load cell that is mounted above the upper supporting arm. The setup is designed to minimize the friction between the specimen and the setup's supports, that is, all four supporting cylinders are
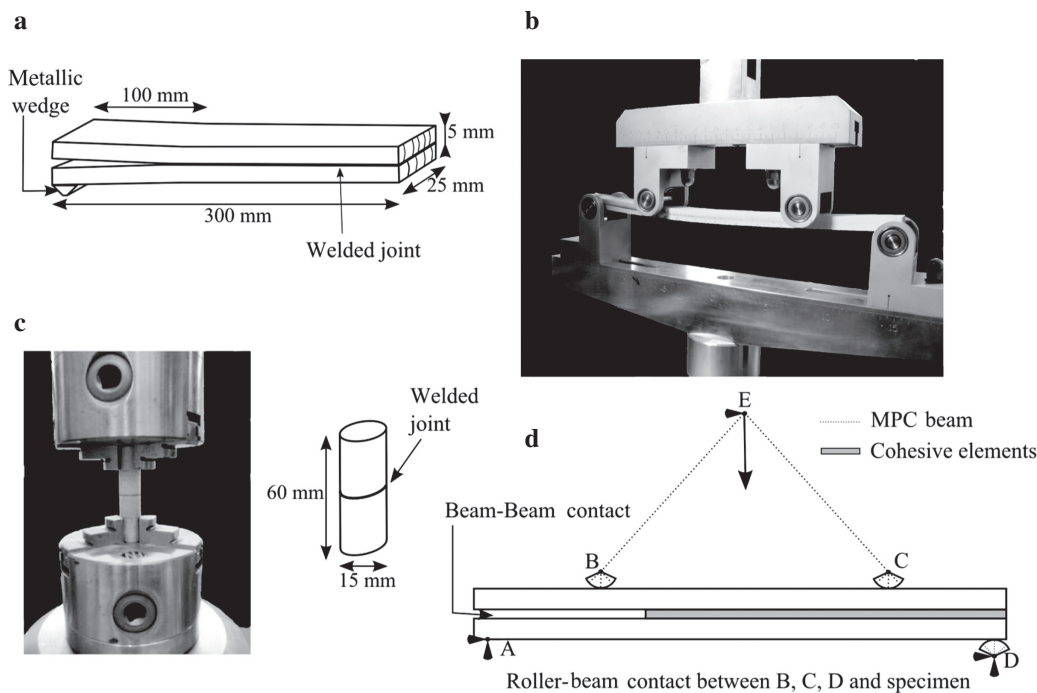

Figure 1 Experimental details.
(a) Sketch of the ENF specimen. (b) Testing fixture of the 4-ENF test. The supports are mounted on rollers bearings. To keep the specimen from moving horizontally, a wedge is glued on the left-hand side (a) of the specimen and fitted in the roller with its pointed edge. A video camera records the pictures of the lateral surface of the joined beams for subsequent evaluation of the crack length. (c) Torsion experiment and geometry of the specimen. (d) Schematic illustration of the experimental configuration for FEM.

mounted on roller bearings. One of the lower supports has been machined to fit the wedge block glued on one of the specimen's beam. Furthermore, to avoid the friction between initial crack faces, a Teflon sheet is inserted in the crack before the test (Figure 1b).

The span between the lower supports is 290 mm long and the span between the upper supports is set equal to one half (i.e., 145 mm). With this configuration, the initial crack tip is located between the two upper supports at a distance of 27.5 mm to the nearest support (i.e., left). The upper part is pushed down at a constant displacement speed of 2 mm min^{-1} and the load and crossbeam displacement were recorded every 2 s. To track the crack advance, a Guppy camera from Allied Vision Technologies (Stadtroda, Germany) with a 50 mm lens is installed and set to take pictures of the lateral marked surface every second.

Torsion testing

The torsion tests were performed on an MTS 809 with an axial-torsional load cell of 10 kN axial load and 100 Nm torque. The specimen is placed in the setup with a distance between the grips of 20 mm and is subsequently loaded at a constant rate of 5° min^{-1} until failure. During the torsional loading, the axial system compensates for displacements in a way that the axial load is zero throughout the test duration. Torque and angle are recorded at 10 Hz frequency. For the setup and specimen configuration, see Figure 1c.

Finite element modeling

The experimental conditions were simulated by means of the software Abaqus/CAE (see also Figure 1d). The problem is considered to be two-dimensional and plane strain and the wood beams are represented with quadratic quadrilateral elements. The glued metallic wedge inserted in the left-hand support is represented by a 10-mm-long node set at the bottom surface of the lower beam. This set is constrained with a multipoint constraint (MPC) to a point in its middle (A) that only has a rotation degree of freedom. The other supports are modeled by disk's sectors filled with quadratic triangle elements. The beam MPCs link the surfaces of the sectors with their centers (B–D). The displacement is imposed on a reference point (E) that is linked to the two upper supports centers by a beam MPC.

The frictionless contacts in the tangential direction and the hard contact in the normal direction were set between the supports and the beams (roller-beam contact) and between the two internal surfaces of the beam (beam-beam contact). In this way, the interpenetration of the different material domains is avoided while simulating a frictionless process. A calculation with penalty tangential behavior and a coefficient of friction μ=0.4 (equivalent to wood-to-wood and wood-to-steel friction) (Dietenberger et al. 1999) was performed.

The expressions of the material properties for the wood beams are the same as those presented in Part 1 (Rhême et al. 2013). The parameters of the cohesive law are determined based on the fracture toughness measured by the 4-ENF test and the ultimate shear strength from the torsion test. In this work, the maximal shear stresses defining the cohesive elements are considered equal in both shear directions (i.e., $t_s^0 = t_t^0$) and are presented together with the value of G_{IIc} in Table 1. The mechanical properties of steel were applied for the supports B–D (i.e., E=210 GPa, ρ=7800 kg m^{-3}, and ν=0.3). The high stiffness of the cohesive elements renders the calculations quite unstable; thus, an explicit formulation was needed to enable an unconditionally stable calculation.

Table 1 Values of the maximal shear strength and critical energy release rate used in the cohesive law for the numerical study.

Parameter	Values at the MC of			
	6.1%	**11.9%**	**16.8%**	**22.1%**
t_s^0 or t_t^0 (MPa)	6.9	5.9	3.8	1.7
$G_{IIc}\left(\dfrac{J}{m^2}\right)$	142	152	124	81

The indicated MCs correspond to the MCs of the 4-ENF specimens.

Results and discussion

Experimental testing

Fracture testing

In the typical load-displacement curves obtained during the 4-ENF test for different MCs (Figure 2), the experimental error is represented by a gray area. This was calculated according to the standard deviation of the experimental curves. The curves can be divided in three zones. At the beginning, there is an elastic loading part, and later, at some critical load, the crack propagation initiates and advances. This step is characterized by an evolution at a nearly constant load. Once the crack tip reaches the location of the second support, the propagation is stopped, and the load starts to increase again. The photographs presented in Figure 3a illustrate the crack propagation. The shear effect is visible by the relative movement of the vertical marking after the crack growth. The crack propagates in the interface between the joint material and the wood with frequent crossing of the welded joint to reach the other interface (Figure 3b). In all cases, the crack advances within the bond without affecting the wood. The fracture surfaces look very similar to those observed in the mode I propagation (Rhême et al. 2013). In the present case, however, the presence of fibers on the splitted bond's surfaces of moist specimens (22% of MC) is much less evident than in the case of mode I fracture. Probably, the translational relative movement of the two surfaces smoothed the pulled-out fibers, which are pressed again into the surface.

Energy release rate calculation

G_{IIc} is expressed by Equation (1):

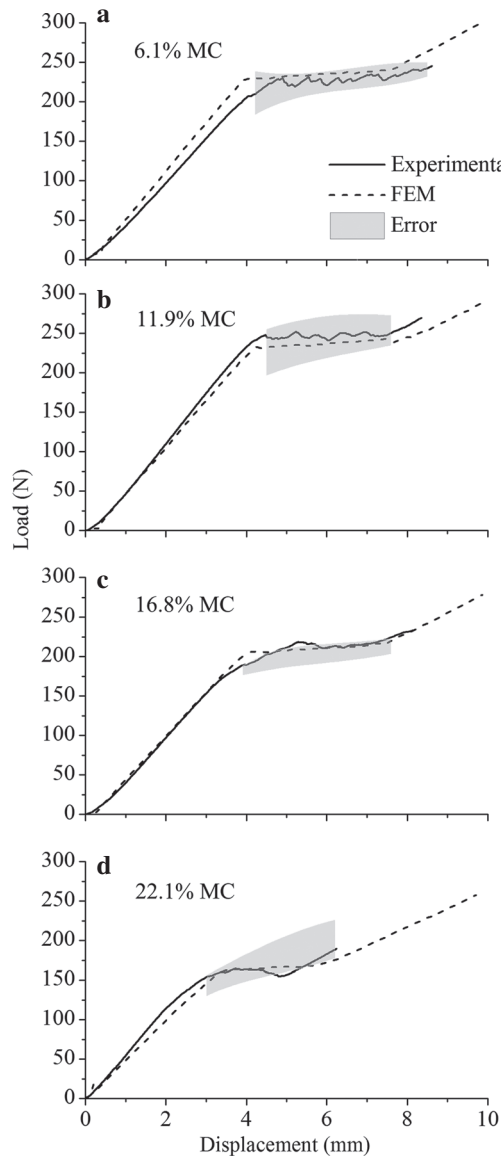$$G_{IIc} = \frac{P^2}{2b}\frac{\partial C(a)}{\partial a} \tag{1}$$

Figure 2 Comparison of typical load-displacement experimental curves (solid line) with data obtained by FEM (dashed line). The gray zone represents the error margins calculated according to the different experimental curves.

where P is the load applied on the specimen during crack propagation, b is the thickness of the specimen, C is the compliance, and a is the crack length.

In the case of a bending test with 4-ENF specimen, the expression of the compliance $C(a)$ in terms of the crack length a can be fitted with a linear expression $C(a)=C_1 a+C_2$. Therefore, the derivative of this last expression with respect to a gives the value of C_1 that is needed to solve Equation (1).

Despite an initial lower value of G_{IIc} calculated at the loss of linearity of the initial part of the load-displacement curve, all further values are nearly constant, within the
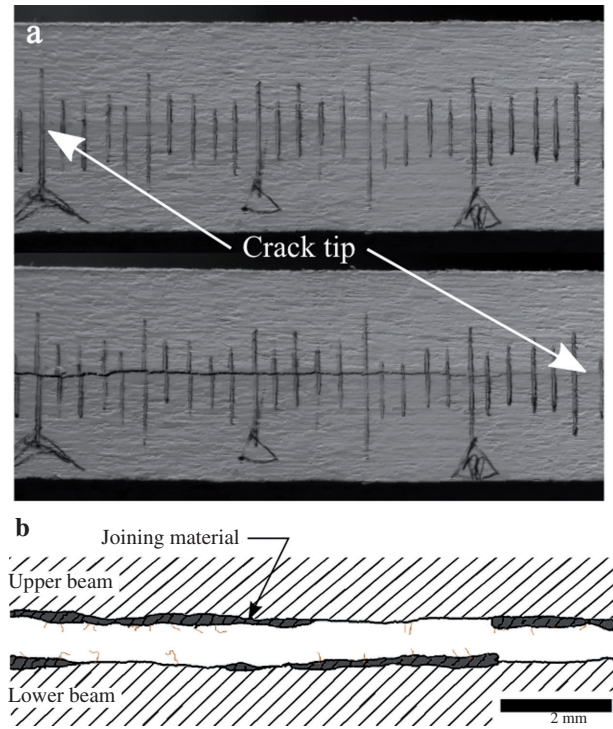

Figure 3 Experiments with ENF specimens.
(a) Photograph at the beginning of the test (top) and after ~25 mm of crack propagation (bottom). The distance between each vertical line is 1 mm. (b) Sketch of the lateral surface of the ENF specimen after separation, which is based on the optical microscopy observations. The dark parts represent the joining material and the wood beam appears striped. Fibers are indicated by the thin lines.

experimental error, and lack of a discernible R-curve behavior. Therefore, as soon as the load plateau is reached, the values of G_{IIc} are taken into account for the calculation of the average. These values of G_{IIc} and their variation with MC are presented in Figure 4 and show a similar trend to that in mode I (Rhême et al. 2013). A small difference
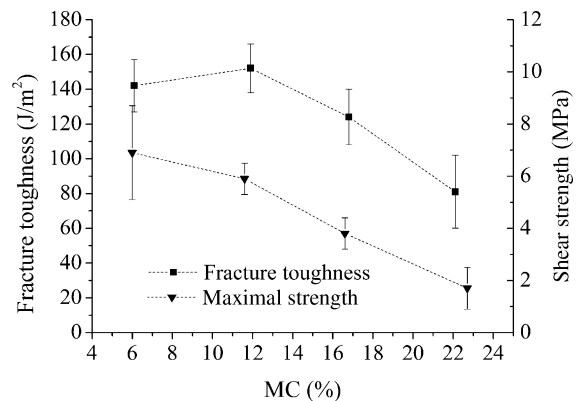

Figure 4 Evolution of the critical energy release rate (G_{IIc}) and the maximal shear strength of the welded joint in as a function of MC of each group of specimens.

of the average values can be noticed between specimens with 6% and 12% MC. However, at MC higher than 12%, the critical energy release rate seems to decrease. The values of G_{IIc} are twice higher than those of G_{Ic}. A comparison with solid wood is difficult because no value of G_{IIc} for beech has been found in the literature. In the mode II fracture of spruce, Yoshihara (2004) introduced grooves on the lateral surfaces to achieve rectilinear crack growth, to lower the load necessary for crack propagation, and therefore to avoid the bending failure of the specimen before crack propagation. In the case of the welded joints, no reduction of the section is necessary for crack propagation in mode II, indicating that the value of G_{IIc} of the joint is probably lower than that of solid wood. For comparison, a few tests have been performed with solid beech wood specimen taken from the same plank, from which welded specimens were produced. Grooves were also necessary to avoid bending failure. Unfortunately, such features prevent observing precisely the crack length; therefore, it is only possible to calculate a G_{IIc} at initiation. At 12% MC, this value is 550 J m^{-2}, which is comparable with spruce (see Yoshihara 2004) and about four times higher than the G_{IIc} of welded joint.

Torsion testing

The typical curves obtained from the torsion tests are presented in Figure 5a for all four different MCs. Moisture led to the decrease in both the angle and the torque at failure. The calculation of the maximal shear strength is approximated with Equation (2):

$$\tau_{max} = \frac{16T}{\pi HB^2},\qquad(2)$$

where T is the torque at failure and H and B are the long and short axis length of the elliptical section, respectively. The maximal shear strengths are plotted in Figure 4 as a function of MC. The error for the dry specimen is relatively large, but a constant decrease of the average values with increasing MC is clearly visible. Three main types of torsion failure are observable. As shown in Figure 5b, failure can occur totally in the joint (most of the time) or partially in the joint and in the wood. This is particularly true for dry specimens (6% and 12% of MC) with a calculated maximal strength in the order of magnitude of the maximal shear strength of beech (Vorreiter 1949; Kollmann 1982). In this work, only the specimens with a total failure in the joint were considered for calculating the average of the shear strength of the joint in Equation (2).

Finite element modeling

The wave propagation solution was required as an explicit formulation, which induces a jagged load-displacement curve in the simulation. The curves shown in Figure 2 (dashed lines) are smoothed with a moving average over 7 points. Interestingly, the finite element model (FEM) curves fall within the range of the experimental data if the experimental errors are taken into consideration. The slope of the initial part of the simulated curves, which correspond to the elastic response of the wood beams, gradually increases with decreasing MC. This clear effect is due to the modulus evolution caused by MC (Dinwoodie 1989). Note that the slopes of the experimental curves for a given MC (not all shown for better clarity) show larger variations due to the natural variability of the wood.

The presented model is sufficiently representative of the reality and seems to be suitable to investigate the
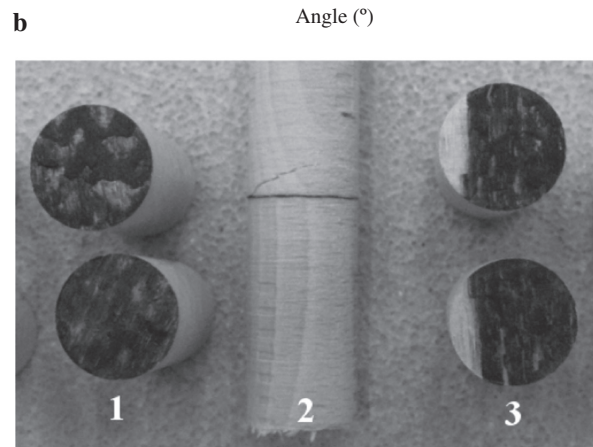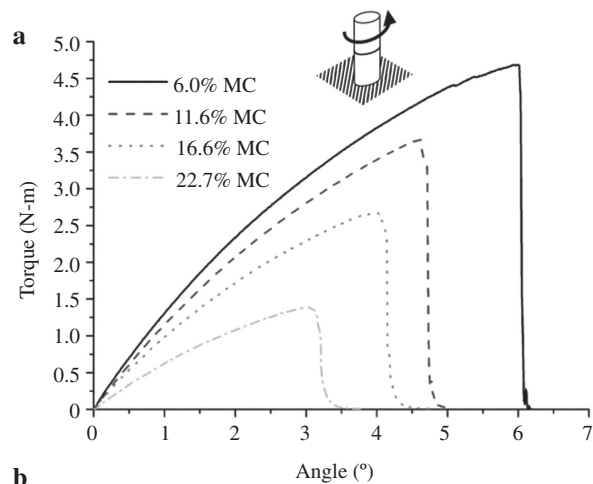

Figure 5 Torsion test.
(a) Torque related to the angle of rotation during the torsion test. One representative curve for each MC is presented. (b) Torsion specimens after fracture. Three types of fracture occurred. (1) Fully in the welded joint, (2) partially in the joint and mainly in wood, and (3) partially in wood and mainly in joint.
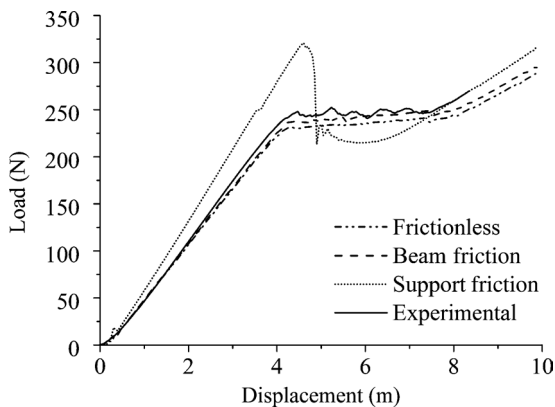
Figure 6 Effect of friction on the load-displacement response according to the FEM.
Friction between the support and the specimen has much more influence than friction between the beams of the specimen. "Beam Friction" is for the friction between the two wood beams. "Support Friction" refers to friction between the supports and the specimen. In both cases, the coefficient of friction was supposed to be $\mu=0.4$.

effects of friction on the test's results. The sources of friction during the test are located either between the two wood beams (i.e., on the crack faces) or between the supports and the specimen. In the simulation reported herein, the coefficient of friction is set to a value 0.4 in both cases of friction, which correspond to either wood-wood or steel-wood friction. Figure 6 shows the effect of friction on the FEM curves, which are compared with the experimental curve of a specimen at 12% MC. The frictionless and beam friction curves are slightly different but still in the range of the variation of the experimental curve. On the contrary, the friction of the supports on the specimen has quite important effects on the load-displacement curve: the initial slope is steeper and the maximal load is

higher. Such a curve would not allow computing a correct G_{IIc}. The setup in this study was effective in eliminating the large parts of the friction.

Conclusion

The 4-points bending of ENF specimens was suitable for the study of the mode II fracture of welded joints. However, the influence of friction must be reduced to a minimum. Otherwise, the friction between the loading support and the specimen may induce important artifacts on the load-displacement data measured. The critical energy release rate and the maximal shear strength have been measured at different MC, and these properties showed a clear decreasing tendency with increasing MC. A numerical study showed that the cohesive elements with a linear damage law are sufficient to model the welded joint.

Both mode I and mode II fractures induce a crack propagation in the joining material and confined between the wood interfaces. Unlike the conventional glues, the joining material does not penetrate the wood; thus, the adhesion is relatively weak in the case of welded joints. Wood cells and the joining material are dissimilar and the external loads weaken the assembly easily. Moreover, the welded connections are very sensitive to moisture.

References

Aicher, S., Boström, L., Gierl, M., Kretschmann, D., Valentin, G. (1997) Determination of fracture energy of wood in mode II. Technical report, RILEM TC 133.

Arrese, A., Carbajal, N., Vargas, G., Mujika, F. (2010) A new method for determining mode II R-curve by the end-notched flexure test. Eng. Fract. Mech. 77:51–70.

Dietenberger, M.A., Green, D.W., Kretschmann, D.E., Hernandez, R. (1999) Wood Handbook—Wood as an Engineering Material. Forest Products Laboratory, Madison, WI.

Dinwoodie, J. (1989) Wood, Nature's Cellular, Polymeric Fibre-Composite. The Institute of Metals, London.

Kollmann, F. (1982) Technologie des Holzes und der Holzwerkstoffe. Springer-Verlag, Berlin.

Kretschmann, D.E., Green, D.W. (1996) Modeling moisture content-mechanical properties relationship for clear southern pine. Wood Fiber Sci. 28:320–337.

Kutnar, A., Kamke, F., Nairn, J., Sernek, M. (2008) Mode II fracture behavior of bonded viscoelastic thermal compressed wood. Wood Fiber Sci. 40:362–373.

Rhême, M., Botsis, J., Cugnoni, J., Navi, P. (2013) Influence of the moisture content on the fracture characteristics of welded wood joint. Part 1: Mode I fracture. Holzforschung 67:747–754.

Schuecker, C., Davidson, B.D. (2000) Evaluation of the accuracy of the four-point bend end-notched flexure test for mode II delamination toughness determination. Compos. Sci. Technol. 60:2137–2146.

Simon, F. (2001) Endommagement et rupture des joints collés sollicités en traction ou cisaillement. Application au collage du bois. Ph.D. thesis, Université Bordeaux I.

Vorreiter, L. (1949) Holztechnologisches Handbuch, Vol. I, Verlag Georg Fromme & Co, Wien.

Yoshihara, H. (2004) Mode II R-curve of wood measured by 4-ENF
    test. Eng. Fract. Mech. 71:2065–2077.
Yoshihara, H. (2005) Mode II initiation fracture toughness analysis for
    wood obtained by 3-ENF test. Comp. Sci. Technol. 65:2198–2207.

Yoshihara, H. (2012) Mode II critical stress intensity factor of wood
    measured by the asymmetric four-point bending test of single-
    edge-notched specimen while considering an additional crack
    length. Holzforschung 66:989–992.